IEEE Access
Multidisciplinary | Rapid Review | Open Access Journal

Received 7 July 2023, accepted 20 July 2023, date of publication 31 July 2023, date of current version 7 August 2023.

Digital Object Identifier 10.1109/ACCESS.2023.3300261

RESEARCH ARTICLE

A Low-Temperature Efficient Approach for the Fabrication of ZnO-rGO heterostructures for Applications in Optoelectronic Applications

REWREWA NARZARY[1], RAJIB CHETIA[2], AND PARTHA PRATIM SAHU[3], (Senior Member, IEEE)

[1]Department of Electronics and Telecommunication Engineering, Jorhat Institute of Science and Technology (JIST), Jorhat, Sotai, Assam 785010, India
[2]Department of Electronics and Communication Engineering, CIT Kokrajhar, BTR, Kokrajhar, Assam 783370, India
[3]Department of Electronics and Communication Engineering, Tezpur University, Napaam, Assam 784028, India

Corresponding author: Rajib Chetia (r.chetia@cit.ac.in)

ABSTRACT In recent years, graphene oxides (GO)/reduced graphene oxide (rGO) and its derivatives have garnered/gained the attention of the scientific and research community due to their superior candidature in various electronic and optoelectronic devices due to their exceptional solution processability, easy fabrication, and tunable electron transport properties. However, the requirement of high-temperature processing steps and complicated processes motivates the scientific community to find simple, efficient, and low-temperature methods. Here, we report the synthesis of GO/rGOs and ZnO-rGO nanocomposite at a relatively low temperature of 150 °C using a simple and efficient solution-processed methodology. The SEM/EDX, XRD, Raman spectroscopy, FTIR, and UV-vis spectroscopy performed to investigate the morphological, structural, and optical properties confirmed the successful synthesis of GO, rGO, and ZnO-rGO with an enhanced carbon-carbon (sp^2 and sp^3) component and reduced oxygen-containing functional group and the restoration of the graphitic domain in the hybrid nanocomposite, attributed to the possible chemical interaction between the rGO and ZnO through oxygen-containing functional groups. The bandgap of ZnO-rGO is modulated from 3.27 eV to 2.72 eV in comparison to pure ZnO. Using Hall measurement the carrier concentration was found to be $3.077 \times 10^{17}cm^{-3}$, $4.518 \times 10^{20}cm^{-3}$, and $2.973 \times 10^{19}cm^{-3}$ for ZnO, rGO, and ZnO-rGO, respectively, and the mobility was calculated as 16.787 cm^2/V.s, 46.112 cm^2/V.s and 25.953 cm^2/V.s, respectively. The fabricated cell exhibited a power conversion efficiency of 6.17 % ($V_{oc} = 0.551$ V and $J_{sc} = 24.33$ mA/cm^2. After 8 weeks, 90 % of the initial efficiency could be achieved, suggesting excellent stability of the fabricated devices. The prepared samples have potential applications in different electronics and optoelectronics devices for enhanced performance.

INDEX TERMS rGOs, ZnO-rGO, nanocomposites, low-temperature, mobility, carrier concentration.

I. INTRODUCTION

This Zinc oxide (ZnO) having a direct bandgap with binding energy ∼ 60 meV, greater than the thermal energy in ambient conditions has been a renewed interest for the scientific research community, mainly triggered by its prospects in electronic and optoelectronic applications [3]. It is considered an encouraging material for structures such as p-n junctions, utilized as a fundamental element in many optoelectronics devices including photovoltaics [5], [6], [7], photodetectors [9], [10], piezoelectric harvesting systems [13], [14], transistors [16], due to having high photoconductivity, radiation hardness, chemical stability and easy fabrication. Extensive reviews are available on the applications of ZnO in various device fabrication [19], [20]. Various strategies have been employed for the fabrication of heterostructures that require very high temperatures, complex and numerous procedures, deposition of multiple layers, by sophisticated and expensive equipment, time-consuming methods such as chemical vapour deposition (CVD) [22], atomic layer

The associate editor coordinating the review of this manuscript and approving it for publication was Shuo Sun.

deposition (ALD) [11], [23], low-pressure CVD (LPCVD) [24], magnetron sputtering [26], etc. The methods also demand the use of potentially hazardous chemicals like hydrofluoric acids (HF) and nitric acids (HNO_3) for surface texturing [1]. In this direction, we worked on the development of ZnO/p-Si heterojunction solar cells using a simple and efficient methodology [5]. ZnO mainly suffers from poor electrical conductivity, low charge carrier mobility, faster recombination, and high lattice thermal conductivity due to having low charge carrier concentration [25], [27]. Al is often used as a dopant to dope ZnO for the formation of $Zn_{(1-x)}Al_xO$. To improve electron transport properties, however, the limited solubility of Al (< 2 atoms) in ZnO limits the further increase in electrical conductivity of the nanostructures [27]. Many strategies have been employed to enhance the electronic transport properties such as hybridization of ZnO with carbon based nanostructures including GO [28], rGO [29], [30], and graphene [31]. However, the high temperature requirement for the preparation of GO and rGO, and the complicated graphene transfer process prompted the research community to find an efficient alternative requiring low-temperature and easy processing steps. In such nanocomposites, Zn^{2+} is collected by rGO and releases excess electrons, responsible for the enhanced electron density as confirmed by Hall measurements. The fabrication of ZnO-rGO nanostructure exhibits many scientific and technological advantages finding application in many electronic and optoelectronic devices including supercapacitors [32], [33], sensors [34], [35], [36], photocatalysis [37], [38], heterojunction solar cells (HJSCs) [25], [39], [40], etc. For this reason, various methodologies including MOCVD [41], PECVD [42], chemical deposition, solvothermal, hydrothermal, precipitation [43], [44], [45], [46], etc. have been envisaged for the fabrication of this nanocomposite. Most of the above-mentioned methodologies are time-consuming, complex processing, expensive, and require highly sophisticated equipment. Therefore, cost-effective and efficient methodologies for the fabrication of ZnO-rGO hybrids to be used in various devices have garnered the attention of the research community due to having many technological advantages. In this direction, we propose the fabrication of ZnO-rGO hybrid nanostructure employing a simple, efficient, and inexpensive solution-processed technique. The carrier concentration, mobility, and simultaneously the electrical and optoelectronic properties of the nanostructure have been modulated by incorporating rGO as confirmed by the Hall Effect and UV-vis measurements. The solution fabrication of hybrid nanostructure/heterostructure with rGOs embedded in ZnO facilitates the formation of a matrix at the molecular level. The findings in the present work can be advantageous for the industrial and the scientific community to tune the performance of the devices by easily modulating the carrier concentration, mobility and simultaneously optimizing the electrical and optoelectronic properties of the heterostructures.

II. EXPERIMENTAL

A. PREPARATION OF GO AND rGO-ZnO HETEROSTRUCTURE

Preparation for GO is discussed elsewhere [47]. For the preparation of ZnO-rGO hybrid semiconductors, 40 ml DI water was taken in a clean beaker. 3.6 g zinc acetate dehydrate ($(Zn(CH_3COO)_2{\cdot}2H_2O)$ was added and stirred for 30 mins, maintaining the temperature at 110 °C. 0.2 ml NaOH (1M) was added to the solution very slowly (drop-wise), raising the temperature to 120 °C, the solution was further stirred for 2 hrs, resulting in a homogeneous milky white solution. 10 ml of the resultant solution was taken in two separate beakers, then 20 ml of ethanol and 100 mg of freshly prepared GO were added to the beaker. After ultrasonication for 5 to 10 mins, the solution was transferred to an autoclave and heated at 150 °C for two different times, 4 hrs and 6 hrs. This process facilitated the simultaneous reduction of graphene oxide with ethanol/thermal reduction and the formation of ZnO-rGO nanocomposites. After cooling down to ambient temperature, the final product was washed multiple times with the aid of centrifugation. The obtained product was then added to a 20 ml PVA dissolved solution, stirred for 15 mins, and coated on a flexible paper substrate with Ag electrode for room temperature. I-V measurement of the prepared samples, followed by drying in an oven at 90 °C for 2 hrs for the successful fabrication of ZnO-rGO heterostructure as shown in Fig.1. The ZnO-rGO-PVA solution was spin-coated on the silicon substrate and the Au electrodes were developed using thermal metallization for the fabrication of the heterojunction solar cells.

B. CHARACTERIZATION

The structure, morphology, chemical states, and elemental composition of the prepared samples were probed using a high resolution scanning electron microscopy (HR-SEM) (SEM, JOEL-JSM6390LV) imaging. The crystalline phase and out-of-plane orientation were investigated using XRD diffractometer, Rigaku (CuKa source; $\lambda = 1.540598$ A°). The Raman spectroscopy was performed by employing a Renishaw basis series micro-spectrometer, excited by 514.5 nm Ar^+ laser source in the range 400 cm^{-1} to 4000 cm^{-1} to study the crystallographic structure. The spectroscopy acquisition was calibrated using a standard Si(100) sample, exhibiting a primary peak at 520 cm^{-1}. To study the chemical bonding and related functional groups in the material, Fourier transformed IR spectroscopy (FTIR) analysis has been performed in the range 4000 cm^{-1} to 400 cm^{-1}. UV-visible spectroscopy has been performed using a UV-vis spectrophotometer (UV-10, Thermo Scientific) to study the optoelectronic properties of the nanostructured semiconductors including transmittance, absorption, and reflectance of the samples in visible and near UV regime as well as for the estimation of the bandgap. Hall measurement was carried out to estimate the carrier concentration and carrier mobility for the prepared samples. The current-voltage (I-V) measurement of the fabricated

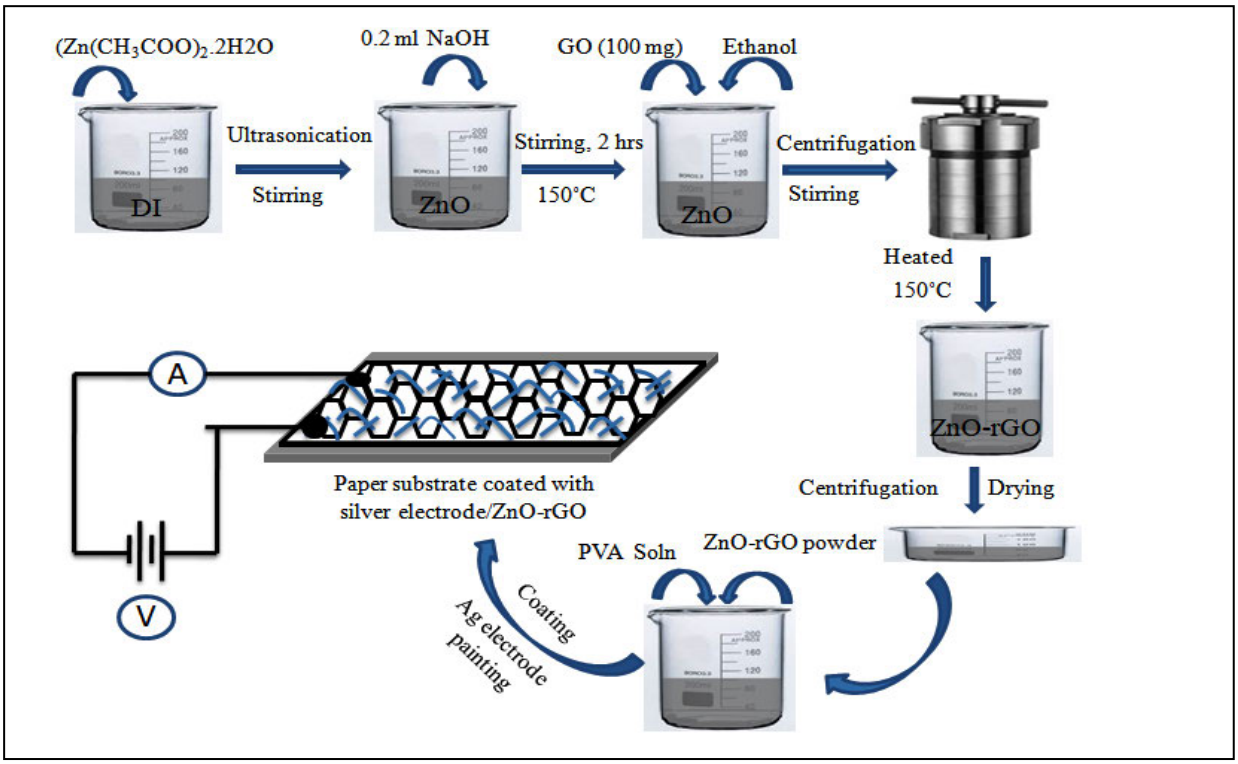

FIGURE 1. Schematic illustration for the preparation of ZnO-rGO nanocomposite and fabrication of Flexible device for I-V characterization.

interdigitated device is performed using an Agilent source (E3631A, 0-5V, 5A/0 - ±25, 1A, triple output). The current density–voltage (*J–V)* curve of the fabricated heterojunction solar cell was the measured sing a computer-controlled Ketley 2400 source meter with an AM1.5 G filter at a calibrated intensity of 100-mW/cm^2 illumination (xenon lamp).

III. RESULTS AND DISCUSSION

A. RAMAN SPECTROSCOPY

The Raman spectra in Fig.2-a shows the D band positioned at 1351 cm^{-1} arising due to the lattice disorder (C-C breathing mode), due to defects and sp^3-like inclusion on oxidation [48], whereas the characteristic G peak at 1588 cm^{-1} is attributed to the highly ordered sp^2 hexagonal graphite lattice. A weak peak at 2700 cm^{-1} is assigned to the 2D peak. The spectrum for rGO (Fig.2-b), exhibits D band at 1346 cm^{-1} and a G band at 1592 cm^{-1} with characteristic peak slightly shifted towards the lower wave number, indicating the successful reduction of GO. It is evident from the result that the ratio of D-band intensity to G-band(I_D/I_G), used to measure the degree of disorder in the sp^2 domain [44], is increased from 0.984 (GO) to 1.109 (rGO), attributed to the reduction of rGO (summarized in Table. 1). For ZnO-rGO hybrid nanocomposite Fig 2 (c & d), the peak located at 420 cm^{-1}, 575 cm^{-1}, and 1165 cm^{-1} is assigned to E_2(high), oxygen deficiency defects in ZnO/E_1(LO), and multiple phonon scattering process/A_1(LO) - E_1(LO) vibration mode due to ZnO nanorods [29], [49]. The spectra also exhibited D band positioned at 1348 cm^{-1} and a G band at 1602 cm^{-1}, demonstrating the preservation of graphitic domain, as supported by FTIR results. The cluster size (L_A) of the as- prepared GO, rGO, and the ZnO-rGO nanocomposite was calculated from the I_D/I_G ratio by using equation (1) [48], and found to be 18.589 nm, 16.495 nm, 16.086/16.108 nm, for GO, rGO, and ZnO-rGO, respectively. The decrease in the sp^2 cluster size through the basal planes in the graphitic domain is attributed to the sp^2 ordering restoration [50].

$$L_A(nm) = 2.4^{*}10^{-10}\lambda^4\frac{I_G}{I_D} \tag{1}$$

where, λ represents the wavelength of the laser and (514.5) nm is used for the laser source Ar^+.

TABLE 1. Showing I_D/I_G ratio of different samples.

Sample	Cluster size L_A (nm)	I_D/I_G ratio
GO	18.589	0.984
rGO	16.495	1.109
ZnO-rGO1	16.086	0.660
ZnO-rGO2	16.108`	0.661

B. FOURIER-TRANSFORM INFRARED SPECTROSCOPY (FTIR) ANALYSIS

The FTIR spectrum of GO (Fig.3 a) exhibits pronounced peak centered at 3400 cm^{-1} which presents the hydrophilic nature

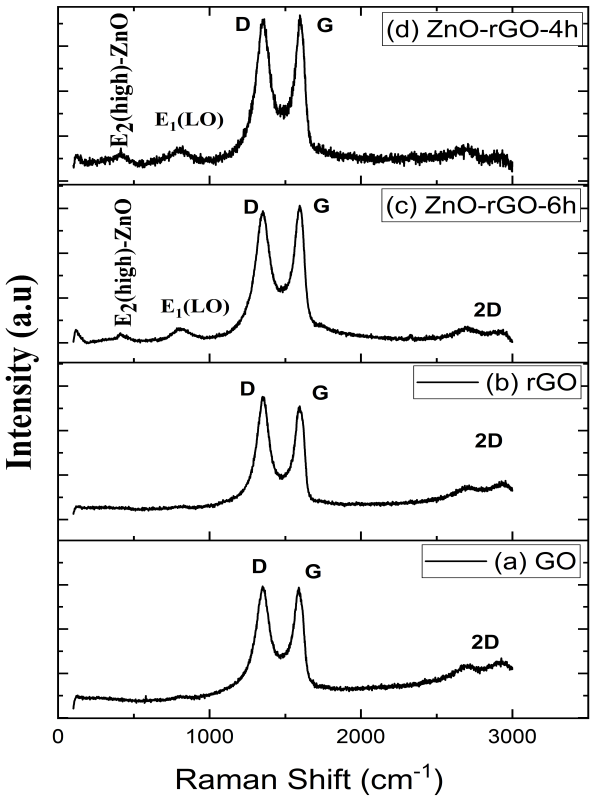

FIGURE 2. Raman spectroscopy of (a) GO, (b) rGO, (c) ZnO-rGO1, (d) ZnO-rGO2.

due to the O-H vibration mode. The spectrum also exhibits the peaks at 1221 cm^{-1}, 1051 cm^{-1}, and at 620-800 cm^{-1}, corresponding to the stretching vibration of carboxyl (C=O), epoxy (C-O-C), and alkoxy (C-O) groups, respectively. The pronounced peak positioned at 1572 cm^{-1} and 1722 cm^{-1} is due to the (C=C) stretching mode. The spectrum also exhibited weak peaks at 2927 cm^{-1} and 2852 cm^{-1} due to the symmetric and asymmetric C-H stretching. In rGO (Fig.3-b), the peaks due to the O-H stretching vibration (3396 cm^{-1}), C-H stretching (2923 cm^{-1}), C=O (1219 cm^{-1}), C-O-C (1052 cm^{-1}), and C-O (511-792 cm^{-1}) reappeared with a significant increase in the carbon-carbon component (sp^2 and sp^3) (1725 cm^{-1} and 1583 cm^{-1}). In the ZnO-rGO nanocomposite Fig.3 (c & d), the broad band centered at around 3400 cm^{-1} is due to the hydroxyl (O-H) stretching, weak peak at 2923 cm^{-1} and 876-1099 cm^{-1} is attributed to C-H stretching and C-O vibration, respectively. The peak at 1725 cm^{-1}, corresponding to C=O does not appear in the nanocomposite samples, indicating the reduction process and the possibility of chemical interaction between rGO and ZnO through the C=O group. Characteristic peaks corresponding to the carbon-carbon aromatic (C=C) group is noticed 1568 cm^{-1} and 1418 cm^{-1}, indicating the restoration of the graphitic domain by the process of reduction. Finally, the characteristic peak positioned at 443 cm^{-1} indexed to Zn-O stretching vibration corresponding to E_{2H} mode of hexagonal ZnO confirms the formation of ZnO-rGO hybrid heterostructure [37], [44].

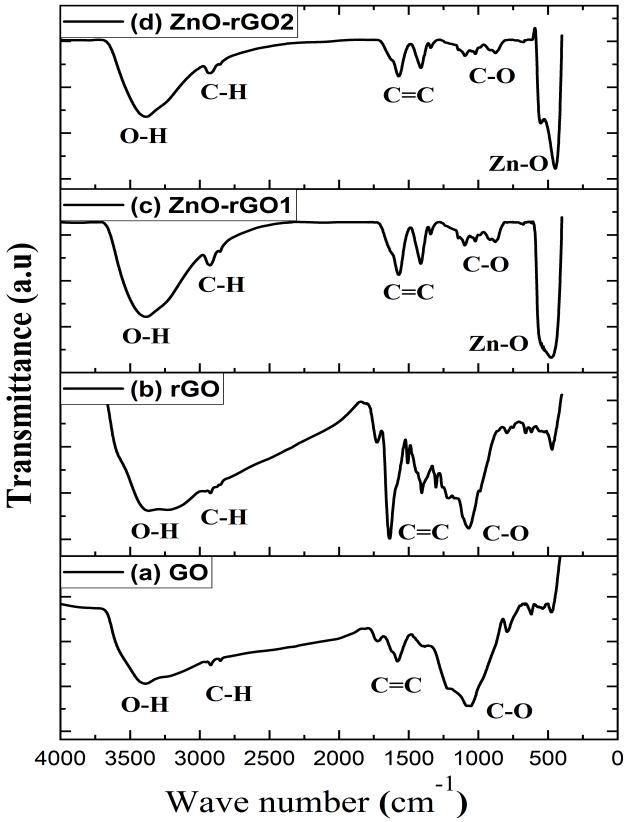

FIGURE 3. FTIR spectra of (a) GO, (b) rGO, (c) ZnO-rGO1, (d) ZnO-rGO2.

C. X-RAY DIFFRACTION ANALYSIS (XRD)

The XRD spectrum of GO (Fig. 4-a), shows a pronounced peak at 2O = 12.80 and 2O = 42.50, indexed to (002) and (100) plane attributed to the carbon atoms. Fig.4 (b), shows the peaks corresponding to rGO with a significant shift towards higher diffraction angle, resulting at around 2O = 26, confirming the successful reduction of GO [51]. In ZnO-rGO samples (Fig. 4 (c & d)), characteristic peaks corresponding to ZnO could be noticed at 2O = 33.07, 35.56, 37.76 and 65.53, indexed to (100), (002), (101) and (103) in case of rGO-ZnO1; and at a diffraction angle of 2O = 31.27, 33.07, 35.66, and 36.80 for rGO-ZnO2, related to hexagonal phases of ZnO. It is observed that the peaks corresponding to rGO are conserved due to the reason that rGO is wrapped or covered with the zinc oxide crystals during the autoclave process. Moreover, rGO is well dispersed in the composite surface, effectively inhibiting the buildup of rGO nanoflakes/nanosheets. To further investigate the crystalline nature of the prepared samples, the average crystal size was computed using the Scherrer's equation given by (D = Kλ/ßcosO) and found to be 45.7 A°, 32.1 A° and 36.9 A for GO, rGO, and ZnO-rGO, respectively.

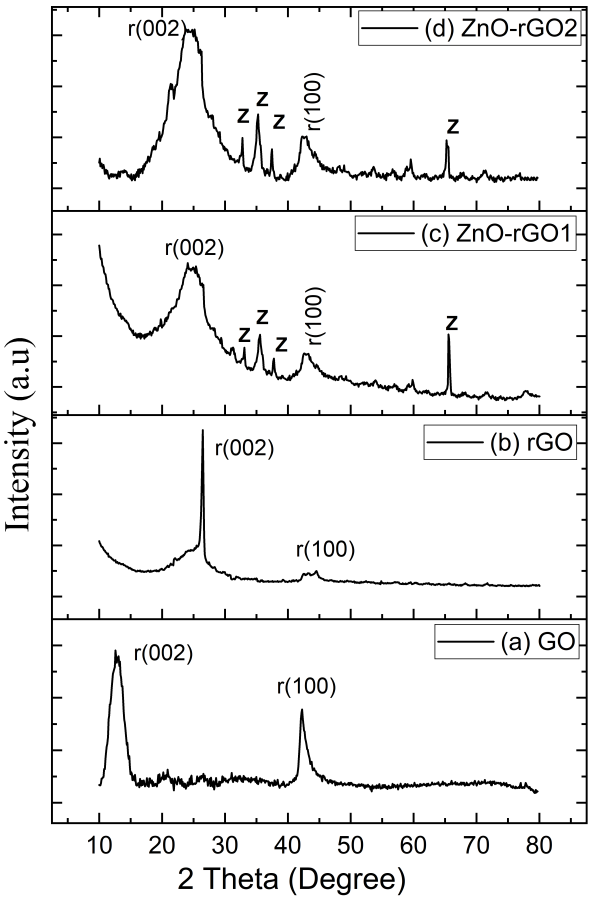

FIGURE 4. XRD spectra of (a) GO, (b) rGO, (c) ZnO-rGO1, (d) ZnO-rGO2.

D. SCANNING ELECTRON MICROSCOPY AND ENERGY DISPERSIVE X-RAY ANALYSIS (SEM/EDX)

Fig. 5 shows the SEM image of the as-prepared GO, rGO, and hybrid rGO-ZnO nanocomposites. Both the size and distribution of the nanostructures greatly depends on the degree of oxidation reaction depending on the synthesis conditions. The size of the nanoflakes/nanorods can be responsible for the degree of carbon-oxygen distribution in the nanostructured materials, a very important factor influencing the optoelectronic properties of the material including, absorption of the spectrum, transmittance, bandgap, and electron transport properties like carrier concentration and mobility of the prepared nanostructures making it a superior candidate in varied electronic and optoelectronic devices, including photodetector, solar cell, sensors, etc. The GO sample (Fig.5-a) exhibited relatively large-sized flakes because of a single-step oxidation process and minimal sonication treatment, and it reduced upon reduction, supporting the EDX result, stating that large-sized flakes absorb more oxygen. It is evident from the SEM micrograph of hybrid ZnO-rGO (Fig.5 (c &d) that zinc oxide nanoparticles/nanorods are incorporated in the rGO nanosheets/nanoflakes. The as-prepared GO carbon-oxygen (C/O) ratio was calculated to be 1.27, with a weight percentage of 56.13 and 43.87 respectively for carbon and oxygen (Table-2). Due to the reduction of as-prepared GO at a low temperature of 150 °C using an autoclave, the carbon to oxygen ratio could be significantly enhanced from 1.21 to 2.41.

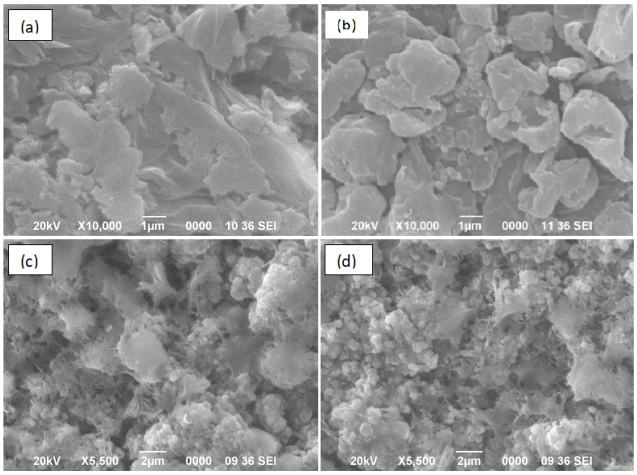

FIGURE 5. SEM micrograph of (a) GO, (b) rGO, (c) ZnO-rGO1, (d) ZnO-rGO2.

TABLE 2. Carbon and oxygen atomic/weight % content of different samples.

Samples	C Weight (%)	O Weight (%)	Zn Weight (%)	C/O Ratio
GO	56.13	43.87	--	1.27
rGO	70.71	29.29	--	2.41
rGO-ZnO1	7.40	16.26	76.34	0.46
rGO-ZnO2	11.27	15.23	73.49	0.74

The variation in the carbon and oxygen content in the sample can facilitate possibility of tuning/modulation of the conductivity, bandgap and other optoelectronic properties of the semiconductor such as carrier concentration and mobility. The ZnO-rGO hybrid heterostructure exhibited a weight percentage of 73.49, 15.23, and 11.27, corresponding to zinc, oxygen, and carbon, respectively, confirming the successful preparation of ZnO-rGO composite semiconductor. The EDX result of GO/rGO and rGO-ZnO samples revealed only the presence of carbon, oxygen, and zinc with varied atomic/weight percentages depending on the synthesis conditions, indicating the formation of relatively pure GO, rGO, and hybrid ZnO-rGO.

E. UV-VIS SPECTROSCOPY ANALYSIS

Fig. 6-a, depicts the UV-vis transmittance spectra of the as-prepared GO, rGO, and the hybrid ZnO-rGO nanocomposites. The result revealed that the transmittance of ZnO nanoparticle/nanorods could be enhanced by the incorporation of rGO, making it a possible potential candidate in

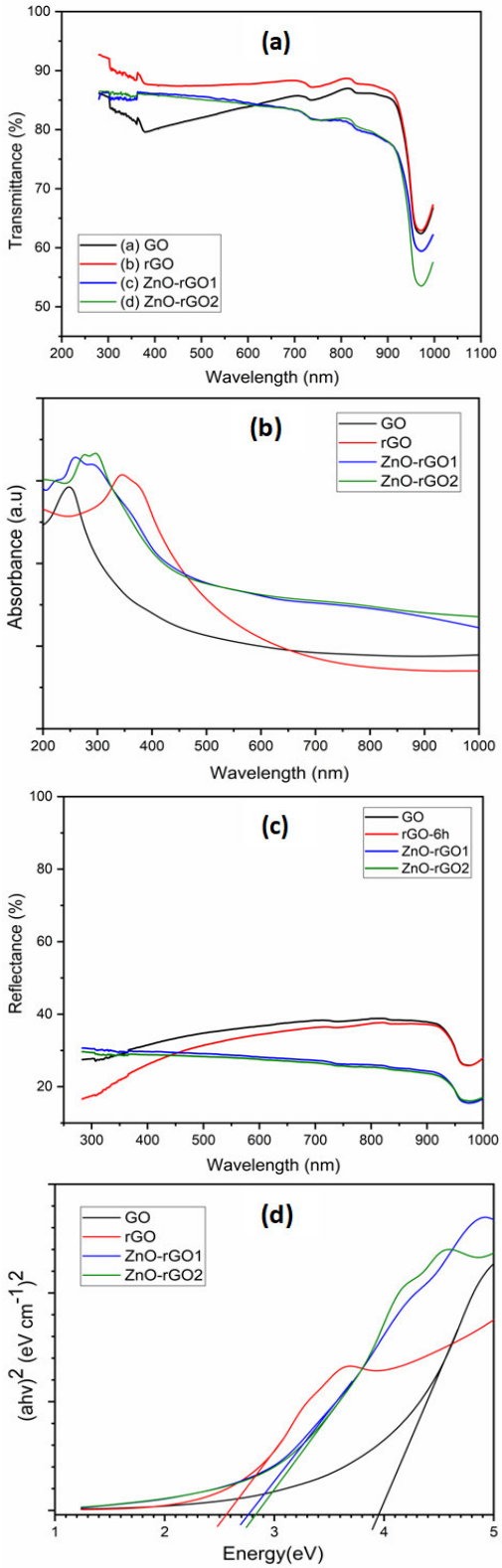

FIGURE 6. (a) UV-vis Transmittance spectra, (b) UV-vis absorption spectra, (c) Reflectance spectra and (d) Taucs plot for the estimation of bandgap of GO, ZnO, rGO, and ZnO-rGO.

optoelectronic devices such as heterojunction solar cells [5], [21] and photodetectors. The UV-vis absorption spectra of the synthesized samples are presented in Fig. 6-b. In GO, an absorption peak is noticed at 236 nm decreasing rapidly in intensity within the visible regime, attributed to the absorption due to GO flakes. For rGO a significant red-shift is noticed resulting in absorption peak at 326 nm. The absorption spectrum of hybrid ZnO-rGO exhibited an absorption peak at 292 nm, and it is to be noted that the hybrid sample significantly absorbs more in the visible spectrum in comparison to pure ones, attributed to the combined absorption due to ZnO nanoparticles/nanorods and the rGO nanoflakes/nanosheets in the ZnO-rGO nanocomposite. In comparison to the pure semiconductors, the percentage reflectance of the ZnO-rGO nanostructured composite in the wavelength range of the visible regime significantly decreased (Fig. 6-c), suggesting the enhanced absorption of incident light, a possible advantage for efficiency enhancement in the case of heterojunction solar cells. The direct bandgap of the prepared semiconductors is calculated using the Taucs equation $(\alpha h\nu)^2 = A(h\nu - Eg)$ [52], [53], by extrapolating the Taucs plot ($(\alpha h\nu)^2$ versus $h\nu$) to the energy axis as shown in Fig.6-d, and found to be 3.95 eV, 2.51 eV, 2.78/2.80 eV, for GO, rGO, and ZnO-rGO, respectively. Regarding the measurement errors, a value of $\pm$ 0.05 eV is assigned for the absolute values of calculated band gaps. The direct bandgap of the prepared semiconductors is calculated using Tauc equation $(\alpha h\nu)^2 = A(h\nu - Eg)$ [52], [53], by extrapolating the Taucs plot ($(\alpha h\nu)^2$ versus $h\nu$) to the energy axis as shown in Fig.6-d, and found to be 3.95 eV, 2.51 eV, 2.78/2.80 eV, for GO, rGO, and ZnO-rGO, respectively. Regarding the measurement errors, a value of $\pm$ 0.05 eV is assigned for the absolute values of calculated band gaps.

F. HALL EFFECT MEASUREMENT OF THE PREPARED SAMPLES

The charge carrier concentration (n) and mobility (μ) of the prepared samples was calculated by Hall measurement using equation (1) and (2), respectively and the important parameters are highlighted in Table 3.

$$n = \frac{IBl}{V_H eA} = \frac{IB}{V_H et} \tag{2}$$

$$\mu = \frac{\sigma}{ne} \tag{3}$$

Here n, I, B, l, V_H, A, e, and t correspond to carrier concentration, current, applied magnetics flux, length, Hall voltage, area, electronic charge, and thickness, respectively. The ZnO nanostructure exhibited a carrier density and mobility of 3.077×10^{17} cm^{-3} and 16.786 cm^2/V.s, respectively. The GO exhibited a carrier concentration of 9.664×10^{15}cm^{-3} and a very low charge mobility of 0.2386 cm^2/V.s. Interestingly upon reduction enhanced carrier concentration and mobility of 4.518×10^{20} cm^{-3} and 46.112 cm^2/V.s could be achieved. In comparison, GO films thermally reduced at an ultrahigh temperature of 2000K achieved a carrier concentration of 1.2×10^{21} cm^{-3} and a mobility of 3.5 cm^2/V.s [54]. Our findings suggest a synthesis of nanostructures with high carrier concentration and high mobility at a relatively low

temperature of 150 °C. High carrier concentration and mobility of the prepared samples suggest the substantial reduction of oxygen containing functional groups, complementing the EDX results. Due to the incorporation of rGO into ZnO to form ZnO-rGO heterostructures a carrier concentration in the order of 10^{19} cm^{-3} and a mobility of 26 cm^2/V.s is obtained. These enhanced electron transport properties of the heterostructure can be very beneficial in many electronic and optoelectronic devices for tuning their performance for enhanced efficiencies.

TABLE 3. Hall Effect measurements showing important parameters.

Samples	Carrier conc. (cm^{-3})	Mobility (cm^2/V.s)	Bandgap (eV)
GO	9.664E15	0.238	3.95
ZnO	3.077E17	16.786	3.27
rGO	4.518E20	46.111	2.50
ZnO-rGO1	1.916E19	26.096	2.78
ZnO-rGO2	2.973E19	25.952	2.72

G. CURRENT-VOLTAGE MEASUREMENT OF THE FABRICATED DEVICES

The Current-Voltage (I-V) characteristics of the fabricated flexible device with ZnO, rGO, and ZnO-rGO nanocomposite sample were measured and presented in Fig. 8. A voltage of -2.5 V to 2.5 V was applied to the electrodes (Ag) of the interdigitated devices and the I-V characteristics were measured in ambient temperature. For the device with GO, the current flowing through the device was negligible ($\sim$ zero) corresponding to the voltage applied. It is noticed that upon reduction the current significantly increased to 8.56 mA attributed to the enhanced carrier concentration and mobility as confirmed by Hall measurement. For the device with ZnO sample a current of 3.41 mA is obtained due to the low charge carrier density and lower electron mobility. When rGO was incorporated into ZnO nanostructure to form ZnO-rGO heterostructure (Fig. 7), a current in the order $\sim$ 5.9 mA was flowing through the device due to the enhanced electron transport properties due to the incorporation of rGO into ZnO nanostructures. The findings suggest the possible application of these heterostructures in various electronic and optoelectronic devices for the enhanced efficiency or performance of the devices.

H. J–V CHARACTERIZATION OF AU/RGO–ZNO/P-Si/AU HETEROJUNCTION SOLAR CELL

Fig. 8 presents the J-V characteristics of the fabricated ZnO/p-Si/Al, ZnO-rGO/p-Si/Au1, and ZnO-rGO/p-Si/Au2 heterojunction solar cells. The ZnO/p-Si/Al solar cell exhibited a PCE of 2.22 % (V_{oc} = 460 mV, J_{sc} = 9.97 mA/cm^2, and FF = 48.40 %) [5]. The efficiency of the ZnO-rGO/p-Si/Au1, and ZnO-rGO/p-Si/Au2 was found to be 6.10 and 6.17, respectively with an open circuit voltage of 0.541 V and short circuit current of 24.52 mA/cm^2 for

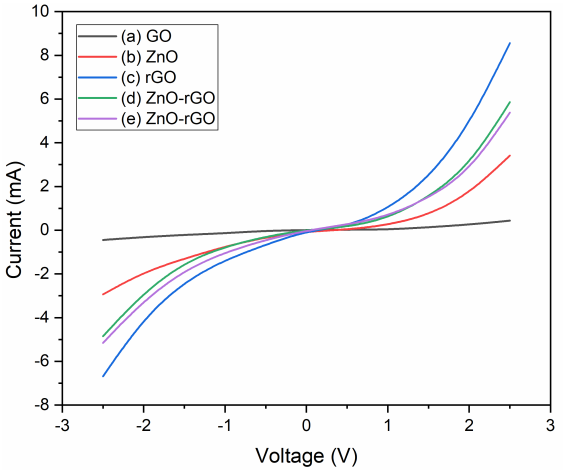

FIGURE 7. Current-Volthage (I-V) characteristics of prepared devices.

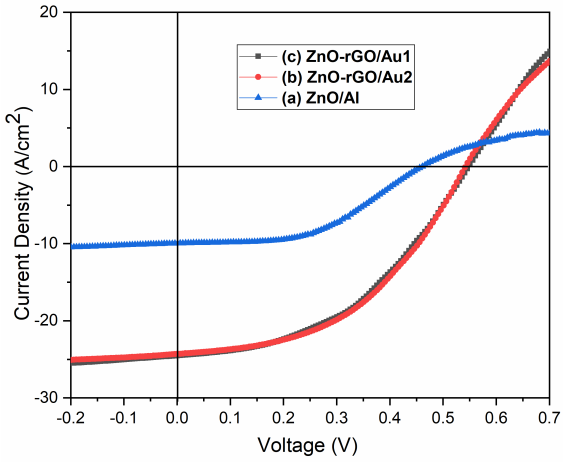

FIGURE 8. J – V characteristics of ZnO/p-Si and hybrid rGO–ZnO/p-Si heterojunction solar cell under AM 1.5 illumination.

ZnO-rGO/p-Si/Au1 and an open circuit voltage of 0.551 V and short circuit current of 24.33 mA/cm^2 for ZnO-rGO/p-Si/Au2. The enhanced efficiency of the developed solar cells is mainly attributed to the enhanced charge carrier concentration and improved mobility of the nanocomposites as confirmed by Hall measurement experiments and the reduced bandgap of the nanocomposites, facilitating reduced photon energy for the generation of free charge carriers. Table 4 highlights some of the recent works reported on ZnO and its composites based heterojunction solar cells. Most of the reported work employed complex and multiple processing steps, used multiple layers, complicated graphene transfer processes, very high temperature requirements, and the use of highly sophisticated instruments/machines thereby resulting to a very high fabrication cost. The performance efficiency of the fabricated devices is comparable to the reported works employing complex processing steps, use of multiple layers, very high temperature requirement, and high cost.

TABLE 4. Recently reported works on ZnO and ZnO based nanocomposites showing the cell parameters.

Device Structure	Fabrication methods	J_{SC} $mAcm^{-2}$	V_{OC} (V)	FF (%)	Ƞ (%)	Refs	Years
Al/p-Si/ZnO-nanoseeds/ZnONRs /ZnO/ZnO-Al	Ultrasonication, ALD Hydrothermal e-beam evaporation	28.4-35.1	0.306-0.435	48-71	4.2-10.9	[1]	2015
Ga-In/Si-MP/GNWs-AgNWs	Si-etching, PECVD (750 ºC) Lithography, e-beam deposition	28.7	0.368	64.4	6.6	[2]	2015
In-Ga/Si/P3HT/PDMS /Gr/Ag	Si-etching, CVD (1040 ºC), Graphene transfer, PMMA etching, LBL method	24.28	0.55	63	8.42	[4]	2015
Ga-In/Si/Al_2O_3/Ag-NWs/Gr/Ag	CVD (1040 ºC), Spincoating Graphene Transfer, ALD	--	--	63	8.68	[8]	2015
Al/Si/$Zn_{(1-x)}Mg_xO$/AZO/Al	Ultrasonication, ALD PVD, e-beam evaporation	34	0.32	66	7.1	[11]	2016
Al/p-Si/ZnO/AgNPs/Al	Sol-gel, Ultrasonication, PLD Spincoating,Thermal evaporation	11.67	0.15	--	3.68	[12]	2017
Al/T-Si/ZnONRs/Ag	Si Texuring, RF sputtering Thermal evaporation Annealing (651 ºC)	2.1-7.30	0.22-0.26	0.44-0.52	2.6-9.1	[15]	2018
Al/Si-nanopillar/ZnO/ITO /Ag	RF magnetron sputtering ICP dry etching, Lithography Thermal evaporation	31.3	~1	39.9	1.20	[17]	2018
Al/FZO/p-Si/A/	Sol-gel, CSP, Ultrasonication Themal evaporation	14.8-23.00	0.46-0.50	48.5-55.3	6.74	[18]	2020
Al/ZnO/p-Si/Al	Sol-gel, thermal oxidation, spin coating, thermal evaporation	6.15-9.97	0.44-0.46	38.7-48.4	2.22	[5]	2020
Au/ZnO-SnO_2/p-Si/Au	Sol-gel, thermal oxidation, spin coating, thermal evaporation	17.71-19.88	0.55-0.58	34.56-36.37	3.39-3.98	[21]	2020
Au/rGO-ZnO/p-Si/Au	Sol-gel, spin coating, thermal evaporation	14.47	0.516	51.60	4.35	[25]	2021
Au/rGO-ZnO/p-Si/Au	Solution process, spin coating, thermal evaporation	24.33	0.551	--	6.17	**This work**	

IV. CONCLUSION

GO has been successfully synthesized using an efficient modified Hummers method. The present work demonstrates a low-temperature efficient fabrication of ZnO-rGO heterostructure, a possible candidate in various optoelectronic applications including heterojunction solar cells and photodetectors. The XRD spectra confirmed the successful preparation of highly crystalline phases of rGO and hybrid nanocomposites. Upon reduction an enhanced carbon-carbon (C=C) (sp^2 and sp^3) graphitic domain could be achieved with above 70 weight percentage of carbon and below 20 weight percentage of oxygen as confirmed from EDX analysis. An increase in the I_D/I_G ratio is also achieved, attributed to the reduction in the defect states and the decrease in the in-plane C=C sp^2 domain. The direct optical bandgap of the prepared nanostructured semiconductors was estimated using Taucs plot and found to be3.95 eV, 2.51 eV, 2.78/2.80 eV, for GO, rGO, and ZnO-rGO, respectively, facilitating a bandgap modulation of the nanostructured semiconductor, a potential for tuning the performance of the device. Hall measurement experiment exhibited a carrier concentration in the range of 9.664E15 cm^{-3} to 4.518E20 cm^{-3} and a mobility of 0.238 cm^2/V.s to 46.111cm^2/V.s.A maximum efficiency of 6.17 %, corresponding to an open circuit voltage of 0.551 V and short circuit current density of 24.33 mA/cm^2 was obtained for the fabricated ZnO-rGO/p-Si/Au1 heterojunction solar cell. After a period of 8 weeks, the fabricated solar cell exhibited power conversion efficiency of 6.10 % that is ∼ 90 % of the initial value, suggesting a good stability of the fabricated devices. These important studies can enable us to tune the electron transport properties as desirable for use in various electronic and optoelectronic devices for the enhanced performance.

ACKNOWLEDGMENT

The authors are thankful to Tezpur University, for providing various facilities for device fabrication and characterization and also thank Palash Phukan, R.S. Department of ECE, Tezpur University for his help during the work.

The author Rewrewa Narzary was with Tezpur University.

REFERENCES

[1] R. Pietruszka, B. S. Witkowski, S. Gieraltowska, P. Caban, L. Wachnicki, E. Zielony, K. Gwozdz, P. Bieganski, E. Placzek-Popko, and M. Godlewski, "New efficient solar cell structures based on zinc oxide nanorods," *Sol. Energy Mater. Sol. Cells*, vol. 143, pp. 99–104, Dec. 2015.

[2] L. Yang, X. Yu, W. Hu, X. Wu, Y. Zhao, and D. Yang, "An 8.68% efficiency chemically-doped-free graphene–silicon solar cell using silver nanowires network buried contacts," *ACS Appl. Mater. Interface*, vol. 7, no. 7, pp. 4135–4141, Feb. 2015.

[3] C. Maragliano, S. Lilliu, M. S. Dahlem, M. Chiesa, T. Souier, and M. Stefancich, "Quantifying charge carrier concentration in ZnO thin films by scanning Kelvin probe microscopy," *Sci. Rep.*, vol. 4, no. 1, pp. 1–7, Feb. 2014.
[4] T. Jiao, J. Liu, D. Wei, Y. Feng, X. Song, H. Shi, S. Jia, W. Sun, and C. Du, "Composite transparent electrode of graphene nanowalls and silver nanowires on micropyramidal Si for high-efficiency Schottky junction solar cells," *ACS Appl. Mater. Interface*, vol. 7, no. 36, pp. 20179–20183, Sep. 2015.
[5] R. Narzary, P. Phukan, S. Maity, and P. P. Sahu, "Enhancement of power conversion efficiency of Al/ZnO/p-Si/Al heterojunction solar cell by modifying morphology of ZnO nanostructure," *J. Mater. Sci., Mater. Electron.*, vol. 31, no. 5, pp. 4142–4149, Mar. 2020.
[6] S. Shoaee, J. Briscoe, J. R. Durrant, and S. Dunn, "Acoustic enhancement of polymer/ZnO nanorod photovoltaic device performance," *Adv. Mater.*, vol. 26, no. 2, pp. 263–268, Jan. 2014.
[7] D. Bi, G. Boschloo, S. Schwarzmüller, L. Yang, E. M. Johansson, and A. Hagfeldt, "Efficient and stable CH_3 NH_3 PbI_3-sensitized ZnO nanorod array solid-state solar cells," *Nanoscale*, vol. 5, no. 23, pp. 11686–11691, 2013.
[8] K. Ruan, K. Ding, Y. Wang, S. Diao, Z. Shao, X. Zhang, and J. Jie, "Flexible graphene/silicon heterojunction solar cells," *J. Mater. Chem. A*, vol. 3, no. 27, pp. 14370–14377, 2015.
[9] T. Chen, X. Gao, J. Zhang, J. Xu, and S. Wang, "Ultrasensitive ZnO nanowire photodetectors with a polymer electret interlayer for minimizing dark current," *Adv. Opt. Mater.*, vol. 8, no. 4, Feb. 2020, Art. no. 1901289.
[10] F. Cao, L. Jin, Y. Wu, and X. Ji, "High-performance, self-powered UV photodetector based on au nanoparticles decorated ZnO/CuI heterostructure," *J. Alloys Compounds*, vol. 859, Apr. 2021, Art. no. 158383.
[11] R. Pietruszka, R. Schifano, T. A. Krajewski, B. S. Witkowski, K. Kopalko, L. Wachnicki, E. Zielony, K. Gwozdz, P. Bieganski, E. Placzek-Popko, and M. Godlewski, "Improved efficiency of n-ZnO/p-Si based photovoltaic cells by band offset engineering," *Sol. Energy Mater. Sol. Cells*, vol. 147, pp. 164–170, Apr. 2016.
[12] P. Shokeen, A. Jain, and A. Kapoor, "Plasmonic ZnO/p-silicon heterojunction solar cell," *Opt. Mater.*, vol. 67, pp. 32–37, May 2017.
[13] J. Briscoe, "Measurement techniques for piezoelectric nanogenerators," *Energy Environ. Sci.*, vol. 6, no. 10, pp. 3035–3045, 2013.
[14] B. Kumar and S.-W. Kim, "Energy harvesting based on semiconducting piezoelectric ZnO nanostructures," *Nano Energy*, vol. 1, no. 3, pp. 342–355, May 2012.
[15] P. Fallahazad, N. Naderi, M. J. Eshraghi, and A. Massoudi, "Combination of surface texturing and nanostructure coating for reduction of light reflection in ZnO/Si heterojunction thin film solar cell," *J. Mater. Sci., Mater. Electron.*, vol. 29, no. 8, pp. 6289–6296, Apr. 2018.
[16] M. Wang, X. Li, X. Xiong, J. Song, C. Gu, D. Zhan, Q. Hu, S. Li, and Y. Wu, "High-performance flexible ZnO thin-film transistors by atomic layer deposition," *IEEE Electron Device Lett.*, vol. 40, no. 3, pp. 419–422, Mar. 2019.
[17] J. Liu, "Fabrication and photovoltaic effect of ZnO/silicon nanopillars heterojunction solar cell," *Microsyst. Technol.*, vol. 24, no. 4, pp. 1919–1923, Apr. 2018.
[18] N. Akçay, "Effect of fluorine doping concentration on efficiency of ZnO/p-Si heterojunction solar cells fabricated by spray pyrolysis," *J. Mater. Sci., Mater. Electron.*, vol. 31, pp. 22467–22477, Nov. 2020.
[19] Ü. Özgür, D. Hofstetter, and H. Morkoç, "ZnO devices and applications: A review of current status and future prospects," *Proc. IEEE*, vol. 98, no. 7, pp. 1255–1268, Jul. 2010.
[20] E. McGlynn, "ZnO nanostructures and their applications," in *Scope: Review, Monograph. Level: Postgraduate, Early Career researcher, Researcher, Specialist, Scientist, Engineers*, X. W. Sun and Y. Yang, Eds. Oxfordshire U.K.: Taylor & Francis, 2013.
[21] R. Narzary, S. Maity, and P. P. Sahu, "Coupled ZnO–SnO_2 nanocomposite for efficiency enhancement of ZnO–SnO_2/p-Si heterojunction solar cell," *IEEE Trans. Electron Devices*, vol. 68, no. 2, pp. 610–617, Feb. 2021.
[22] Y. Zhao, C. Li, M. Chen, X. Yu, Y. Chang, A. Chen, H. Zhu, and Z. Tang, "Growth of aligned ZnO nanowires via modified atmospheric pressure chemical vapor deposition," *Phys. Lett. A*, vol. 380, no. 47, pp. 3993–3997, Dec. 2016.
[23] C.-H. Zhai, R.-J. Zhang, X. Chen, Y.-X. Zheng, S.-Y. Wang, J. Liu, N. Dai, and L.-Y. Chen, "Effects of Al doping on the properties of ZnO thin films deposited by atomic layer deposition," *Nanosc. Res. Lett.*, vol. 11, no. 1, pp. 1–8, Dec. 2016.
[24] N. Aqab, H. Riaz, and A. Nayfeh, "Aluminum doped zinc oxide-silicon heterojunction solar cell by low temperature atomic layer deposition," in *Proc. IEEE 43rd Photovoltaic Spec. Conf. (PVSC)*, Jun. 2016, pp. 598–601.
[25] R. Narzary, P. Phukan, and P. P. Sahu, "Efficiency enhancement of low-cost heterojunction solar cell by the incorporation of highly conducting rGO into ZnO nanostructure," *IEEE Trans. Electron Devices*, vol. 68, no. 7, pp. 3238–3245, Jul. 2021.
[26] L. Shen, Z. Q. Ma, C. Shen, F. Li, B. He, and F. Xu, "Studies on fabrication and characterization of a ZnO/p-Si-based solar cell," *Superlattices Microstruct.*, vol. 48, no. 4, pp. 426–433, Oct. 2010.
[27] D. Chen, Y. Zhao, Y. Chen, B. Wang, H. Chen, J. Zhou, and Z. Liang, "One-step chemical synthesis of ZnO/graphene oxide molecular hybrids for high-temperature thermoelectric applications," *ACS Appl. Mater. Interface*, vol. 7, no. 5, pp. 3224–3230, Feb. 2015.
[28] H. P. Kim, A. R. B. M. Yusoff, and J. Jang, "Organic solar cells using a reduced graphene oxide anode buffer layer," *Sol. Energy Mater. Sol. Cells*, vol. 110, pp. 87–93, Mar. 2013.
[29] A. S. Merlano, L. M. Hoyos, G. J. Gutiérrez, M. A. Valenzuela, and Á. Salazar, "Effect of zn precursor concentration in the synthesis of rGO/ZnO composites and their photocatalytic activity," *New J. Chem.*, vol. 44, no. 45, pp. 19858–19867, 2020.
[30] P. Van Tuan, T. T. Phuong, V. T. Tan, S. X. Nguyen, and T. N. Khiem, "In-situ hydrothermal fabrication and photocatalytic behavior of ZnO/reduced graphene oxide nanocomposites with varying graphene oxide concentrations," *Mater. Sci. Semicond. Process.*, vol. 115, Aug. 2020, Art. no. 105114.
[31] Z. Liu, J. Li, and F. Yan, "Package-free flexible organic solar cells with graphene top electrodes," *Adv. Mater.*, vol. 25, no. 31, pp. 4296–4301, Aug. 2013.
[32] J. Jayachandiran, J. Yesuraj, M. Arivanandhan, A. Raja, S. A. Suthanthiraraj, R. Jayavel, and D. Nedumaran, "Synthesis and electrochemical studies of rGO/ZnO nanocomposite for supercapacitor application," *J. Inorganic Organometallic Polym. Mater.*, vol. 28, no. 5, pp. 2046–2055, Sep. 2018.
[33] M. Ghorbani, M. R. Golobostanfard, and H. Abdizadeh, "Flexible freestanding sandwich type ZnO/rGO/ZnO electrode for wearable supercapacitor," *Appl. Surf. Sci.*, vol. 419, pp. 277–285, Oct. 2017.
[34] P. Cao, Y. Cai, D. Pawar, S. T. Navale, C. N. Rao, S. Han, W. Xu, M. Fang, X. Liu, Y. Zeng, W. Liu, D. Zhu, and Y. Lu, "Down to ppb level NO_2 detection by ZnO/rGO heterojunction based chemiresistive sensors," *Chem. Eng. J.*, vol. 401, Dec. 2020, Art. no. 125491.
[35] P. S. Shewale and K.-S. Yun, "Synthesis and characterization of Cu-doped ZnO/RGO nanocomposites for room-temperature H2S gas sensor," *J. Alloys Compounds*, vol. 837, Oct. 2020, Art. no. 155527.
[36] P. Cao, Y. Cai, D. Pawar, S. Han, W. Xu, M. Fang, X. Liu, Y. Zeng, W. Liu, Y. Lu, and D. Zhu, "Au@ZnO/rGO nanocomposite-based ultra-low detection limit highly sensitive and selective NO_2 gas sensor," *J. Mater. Chem. C*, vol. 10, no. 11, pp. 4295–4305, 2022.
[37] P. Kumbhakar, A. Pramanik, S. Biswas, A. K. Kole, R. Sarkar, and P. Kumbhakar, "In-situ synthesis of rGO-ZnO nanocomposite for demonstration of sunlight driven enhanced photocatalytic and self-cleaning of organic dyes and tea stains of cotton fabrics," *J. Hazardous Mater.*, vol. 360, pp. 193–203, Oct. 2018.
[38] P. Raizada, A. Sudhaik, and P. Singh, "Photocatalytic water decontamination using graphene and ZnO coupled photocatalysts: A review," *Mater. Sci. Energy Technol.*, vol. 2, no. 3, pp. 509–525, Dec. 2019.
[39] K. Yang, C. Xu, L. Huang, L. Zou, and H. Wang, "Hybrid nanostructure heterojunction solar cells fabricated using vertically aligned ZnO nanotubes grown on reduced graphene oxide," *Nanotechnology*, vol. 22, no. 40, Oct. 2011, Art. no. 405401.
[40] P. S. Khare, R. Yadav, and A. Swarup, "RGO-ZnO nanocomposit material of enhanced absorbance for solar energy conversion," *Int. J. Appl. Phys. Math.*, vol. 3, pp. 95–97, Mar. 2013.
[41] J. M. Lee, Y. B. Pyun, J. Yi, J. W. Choung, and W. I. Park, "ZnO nanorod–graphene hybrid architectures for multifunctional conductors," *J. Phys. Chem. C*, vol. 113, no. 44, pp. 19134–19138, Nov. 2009.
[42] W. T. Zheng, Y. M. Ho, H. W. Tian, M. Wen, J. L. Qi, and Y. A. Li, "Field emission from a composite of graphene sheets and ZnO nanowires," *J. Phys. Chem. C*, vol. 113, no. 21, pp. 9164–9168, May 2009.

[43] S. K. Mandal, K. Dutta, S. Pal, S. Mandal, A. Naskar, P. K. Pal, T. S. Bhattacharya, A. Singha, R. Saikh, S. De, and D. Jana, "Engineering of ZnO/rGO nanocomposite photocatalyst towards rapid degradation of toxic dyes," *Mater. Chem. Phys.*, vol. 223, pp. 456–465, Feb. 2019.
[44] T. N. Reddy, J. Manna, and R. K. Rana, "Polyamine-mediated interfacial assembly of rGO-ZnO nanostructures: A bio-inspired approach and enhanced photocatalytic properties," *ACS Appl. Mater. Interface*, vol. 7, no. 35, pp. 19684–19690, Sep. 2015.
[45] A. Shanmugasundaram, R. Boppella, Y.-J. Jeong, J. Park, Y.-B. Kim, B. Choi, S. H. Park, S. Jung, and D.-W. Lee, "Facile in-situ formation of rGO/ZnO nanocomposite: Photocatalytic remediation of organic pollutants under solar illumination," *Mater. Chem. Phys.*, vol. 218, pp. 218–228, Oct. 2018.
[46] P. G. Ramos, E. Flores, C. Luyo, L. A. Sánchez, and J. Rodriguez, "Fabrication of ZnO-RGO nanorods by electrospinning assisted hydrothermal method with enhanced photocatalytic activity," *Mater. Today Commun.*, vol. 19, pp. 407–412, Jun. 2019.
[47] R. Narzary, P. Phukan, S. Das, and P. P. Sahu, "Flexibility of key electronic and optical properties of reduced graphene oxide through its controlled synthesis," *IEEE Trans. Electron Devices*, vol. 69, no. 11, pp. 6400–6407, Nov. 2022.
[48] A. C. Ferrari and D. M. Basko, "Raman spectroscopy as a versatile tool for studying the properties of graphene," *Nature Nanotechnol.*, vol. 8, no. 4, pp. 235–246, Apr. 2013.
[49] S. R. Gollu, R. Sharma, G. Srinivas, S. Kundu, and D. Gupta, "Incorporation of silver and gold nanostructures for performance improvement in P3HT: PCBM inverted solar cell with rGO/ZnO nanocomposite as an electron transport layer," *Organic Electron.*, vol. 29, pp. 79–87, Feb. 2016.
[50] S. Gupta, P. Joshi, and J. Narayan, "Electron mobility modulation in graphene oxide by controlling carbon melt lifetime," *Carbon*, vol. 170, pp. 327–337, Dec. 2020.
[51] P. Phukan, R. Narzary, and P. P. Sahu, "A green approach to fast synthesis of reduced graphene oxide using alcohol for tuning semiconductor property," *Mater. Sci. Semicond. Process.*, vol. 104, Dec. 2019, Art. no. 104670.
[52] Z. K. Bolaghi, S. M. Masoudpanah, and M. Hasheminiasari, "Photocatalytic activity of ZnO/RGO composite synthesized by one-pot solution combustion method," *Mater. Res. Bull.*, vol. 115, pp. 191–195, Jul. 2019.
[53] S. M. Baizaee, M. Arabi, and A. R. Bahador, "A simple, one-pot, low temperature and pressure route for the synthesis of RGO/ZnO nanocomposite and investigating its photocatalytic activity," *Mater. Sci. Semicond. Process.*, vol. 82, pp. 135–142, Aug. 2018.
[54] Y. Wang, Y. Chen, S. D. Lacey, L. Xu, H. Xie, T. Li, V. A. Danner, and L. Hu, "Reduced graphene oxide film with record-high conductivity and mobility," *Mater. Today*, vol. 21, no. 2, pp. 186–192, Mar. 2018.

REWREWA NARZARY received the B.Tech. degree from the Department of Electronics and Communication Engineering, Central Institute of Technology (CIT) Kokrajhar, India, in 2013, and the M.Tech. degree in electronics design and technology (ELDT) and the Ph.D. degree in engineering from Tezpur University, Assam, India, in 2015. He is currently an Assistant Professor with the Department of Electronics and Telecommunication Engineering, Jorhat Institute of Science and Technology (JIST), Jorhat, Sotai, Assam, India. He has published over ten articles in peer-reviewed international journals. His research interests include semiconductor materials synthesis and characterization, heterojunction solar cells, and sensors.

RAJIB CHETIA received the M.Tech. degree in electronics design and technology and the Ph.D. degree in engineering from Tezpur University, Assam, India, in 2001. He is currently an Assistant Professor with the Department of Electronics and Communication Engineering, Central Institute of Technology (CIT) Kokrajhar, India. He has published three articles in peer-reviewed international journals and two international conference proceedings papers. His research interests include semiconductor materials, quantum computation, quantum information processing, and quantum image processing.

PARTHA PRATIM SAHU (Senior Member, IEEE) received the M.Tech. degree from the Indian Institute of Technology, Delhi, and the Ph.D. degree in engineering from Jadavpur University. In 1991, he joined Haryana State Electronics Development Corporation Ltd., where he has been engaged in research and development works related to optical fiber components and telecommunication instruments. In 1996, he joined the North Eastern Regional Institute of Science and Technology, as a Faculty Member. He is currently a Faculty Member with the Department of Electronics and Communication Engineering, Tezpur University, India. He has published more than 98 articles in peer-reviewed international journals, eight books, and 64 international conference proceedings papers. He has three patents on his credit. His research interests include integrated optics and electronic circuits, wireless and optical communication, clinical instrumentation, and quantum communication. He is a Distinguished Fellow of the Optical Society of India and a Life Member of the Indian Society for Technical Education. He received the prestigious INSA Teacher Award from the Indian National Science Academy.